IN VIVO PRECLINICAL MOLECULAR IMAGING OF REPEATED EXPOSURE TO AN NMDA ANTAGONIST AND A GLUTAMINASE INHIBITOR AS POTENTIAL GLUTAMATERGIC MODULATORS.

Stijn Servaes[1], Firat Kara[2], Dorien Glorie[1], Sigrid Stroobants[1,3], Annemie Van Der Linden[2], Steven Staelens[1,*]

---

[1] *Molecular Imaging Center Antwerp (MICA), University of Antwerp, Universiteitsplein 1, 2610, Wilrijk, Antwerp, BELGIUM*

[2] *Bio-Imaging Lab (BIL), University of Antwerp, Universiteitsplein 1, 2610, Wilrijk, Antwerp, BELGIUM*

[3] *Department of Nuclear Medicine, University Hospital Antwerp, Wilrijkstraat 10, 2650, Edegem, Antwerp, BELGIUM*

[*] *Corresponding author*

All correspondence to Steven Staelens: steven.staelens@uantwerpen.be
Molecular Imaging Center Antwerp (MICA), University of Antwerp, Universiteitsplein 1, 2610, Wilrijk, Antwerp, BELGIUM

Financial support

Running title: In Vivo Molecular Imaging of glutamate modulating drugs

Stijn Servaes, Firat Kara, Dorien Glorie, Sigrid Stroobants, Annemie Van Der Linden[2], Steven Staelens[*]

[*] *Corresponding author*

All correspondence to Steven Staelens: steven.staelens@uantwerpen.be

Pages	30 + 6 supplementary
Tables	1
Figures	6
References	34 + 8 supplementary

Wordcount

Abstract:	225
Introduction:	742
Discussion:	788

Abbreviations

2D-OSEM	2-dimensional ordered subset expectation maximization
AMPA	Alpha-amino-3-hydroxy-5-methyl-4-isoxazolepropionic acid
cAMP	Cyclic adenosine monophosphate
CRLB	Cramér-Rao lower bounds
GABA	γ-aminobutyric acid
GLAST	Glial glutamate and aspartate transporter
GLT	Glial glutamate transporter
mGluR	Metabotropic G protein-coupled glutamate receptors
MRS	Magnetic Resonance Spectroscopy
NMDA	N-methyl-D-aspartate
OCD	Obsessive Compulsive Disorder
PET	Positron Emission Tomography
QP	Quinpirole
RARE	Rapid acquisition and relaxation enhancement
TCA	Tricarboxylic acid
KO	Knock-out
IHC	Immunohistochemistry
CT	Computed Tomography
PC	Personal Computer
RARE	Rapid Acquisition with Refocusing Echoes
VOI	Volume of Interest
TAC	Time Activity Curve
SRTM	Simplified Reference Tissue Model

CB	Cerebellum
BPnd	Binding Potential
SPM	Statistical Parametric Mapping
CP	Caudate Putamen
CR	Creatine
PCr	Phosphocreatine
Glc	Glucose
Glu	Glutamate
Gln	Glutamine
GSH	Glutathione
GPC	Glycerophosphorylcholine
PCh	Phosphorylcholine
Ins	Inositol
NAA	N-acetylaspartate
NAAG	N-acetylaspartylglutamate
Tau	Taurine
ROI	Region of Interest

Abstract

Glutamate is the principal excitatory neurotransmitter in the brain and at the base of a wide variety of neuropathologies, including epilepsy, autism, Fragile X and obsessive compulsive disorder. Glutamate has so become the target for novel drugs in treatment and in fundamental research settings. However, much remains unknown on the working mechanisms of these drugs and the effects of chronic administration on the glutamatergic system. This paper investigates the chronic effects of two glutamate modulating drugs with imaging techniques to further clarify their working mechanisms for future research opportunities. Animals were exposed to either Saline (1 mL/kg), MK-801 (0.3 mg/kg) or Ebselen (10 mg/kg) for 7 consecutive days. At the 6th injection, animals underwent a PET/CT with ABP-688 to visualize the mGluR5 receptor. After the 7th injection, animals underwent an MRS scan to visualize Glutamate and Glutamine content. Afterwards, results were verified by mGluR5 immunohistochemistry (IHC). PET/CT analysis revealed that animals receiving receiving chronic MK-801 or Ebselen had a significant ($p<0.05$) higher BPnd (respectively 2.90±0.47 and 2.87±0.46) when compared to Saline (1.97±0.39) in the caudate putamen. This was confirmed by mGluR5 IHC with 60.83%±6.30% of the area being highlighted for Ebselen and 57.14%±9.23% for MK-801 versus 50.21%±5.71% for the saline group. MRS displayed significant changes on glutamine level, when comparing chronic Ebselen (2.20±0.40 µmol/g) to Control (2.72±0.34 µmol/g). Therefore, although no direct effects on glutamate were visualized, the changes in glutamine suggest changes in the total glutamate-glutamine pool. This highlights the potential of both drugs to modulate glutamateric pathologies.

1. Introduction

Glutamate is the principal excitatory neurotransmitter in the brain. It is transmitted via three families of ionotropic receptors, which have intrinsic cation permeable channels (NMDA, AMPA and kainite). Second, there are three groups of metabotropic receptors (mGluR) that act on membrane ion channels and second messengers such as cyclic adenosine monophosphate (cAMP) and diacylglycerol to modify neuronal and glial excitability. Additionally there are three neuronal glutamate transporters in the brain, and two glial glutamate transporters, the Glial glutamate and aspartate transporter (GLAST) and the Glial glutamate transporter (GLT) (Meldrum, 2000).

It has been shown that over-stimulation of the glutamatergic neurotransmission is neurotoxic (Porciúncula *et al.*, 2001) and glutamate abnormalities have been well characterised in a number of neuropathologies such as Fragile X, autism, schizophrenia and epilepsy. Also in other disorders such as depression, anxiety and more recently Obsessive Compulsive disorder (OCD), the emerging role of glutamate signaling has been garnering interest (Coyle, 2006; Pittenger *et al.*, 2011; Miladinovic *et al.*, 2015). Also our group has previously shown that there is a role for glutamate in the quinpirole (QP) rodent model of OCD. In this model, animals are exposed to injections of QP and an Open Field Test on a biweekly basis for a total duration of 5 weeks. These animals show excessive compulsive behavior and were also characterized by an increased distribution of mGluR5, as visualised by PET (Servaes *et al.*, 2017). Another group showed that in Sapap3 KO mice, another preclinical model for OCD (Welch *et al.*, 2007), that mGluR5 signalling was elevated and associated with constitutively active post synaptic receptors (Ade *et al.*, 2016). As it is widely accepted that OCD results from a dysfunctional cortico-striato-thalamical circuitry (figure 1) (Denys *et al.*, 2010),

it is possible that, because the brain is exposed to higher levels of glutamate in OCD patients (Chakrabarty *et al.*, 2005), the normal feedback loop is disrupted. Whether this is a consequence or a cause of the symptoms yet remains to be elucidated. Also in other glutamate related pathologies, such as Fragile X syndrome, autism and epilepsy, there appears to be a specific role for the mGluR5 receptor (Pop *et al.*, 2014; Chana *et al.*, 2015; Kelly *et al.*, 2018).

Taken together, glutamate has so become a target for novel drugs. Therefore, drugs that can interact with the glutamatergic transmission, directly affecting the glutamate levels or the associated receptors in a positive or negative direction, could be of great assistance to further understand these pathologies. By modifying the glutamatergic system in either direction in a preclinical setting, more insight could be acquired in the manifestation of the pathologies mentioned before, either improving or aggrevating the symptoms.

A variety of drugs interact with the glutamatergic system. Ebselen (2-phenyl-1,2-benzisoselenazol-3(2H)-one) is a seleno-organic compound of low toxicity that is characterised by a unique pharmacological profile (Schewe, 1995). There is direct interaction of Ebselen with the glutamatergic system in rats (Nogueira *et al.*, 2002). Although the exact mechanism of action has not been described yet (Azad and Tomar, 2014), preliminary results indicate that Ebselen provides a protection for neurons to ischemic damage (Seo *et al.*, 2009). Furthermore, in vitro studies have shown that Ebselen inhibited [^{3}H]glutamate release and uptake (Porciúncula *et al.*, 2001). Importantly, Ebselen is also an effective glutaminase inhibitor (Thomas *et al.*, 2013).

With glutaminase catalysing the hydrolysis of glutamine to glutamate, this is a further indication of the direct effects of Ebselen on the glutamateric signal.

Another major group of glutamate-affecting drugs targets the NMDA ionotropic glutamate receptor. NMDA receptors play a role in a variety of glutamate-associated pathologies such as OCD (Arnold *et al.*, 2004; Albelda *et al.*, 2010), epilepsy (Ghasemi and Schachter, 2011) and autism (Lee *et al.*, 2015). By directly modulating the NMDA receptors with NMDA receptor antagonists such as ketamine and (+)-MK-801 (dizocilpine maleate), the interneuron GABAergic receptors can be inhibited, which typically results in strong psycho-stimulatory and psychotomimetic effects. Furthermore, this modification could prove to be useful for investigating the NMDA abnormalities on the level of the receptor in the diseases mentioned earlier..

Ebselen's glutamate reducing properties, together with its glutaminase inhibition and protection of ischemic damage, highlight its application potential for OCD. Additionally, although MK-801 will unlikely end up being a treatment option, its possibility to modulate glutamate levels could be of particular importance to further elucidate the underlying glutamatergic role in the QP-induced OCD rats. Previously MK-801 has been used in animal models for OCD to document the effect of activation of NMDA-receptors on the compulsions. Shannon and Love reported that MK-801 increased the rate of lever pressing in rats (Shannon and Love, 2004). In another animal model, MK-801 aggravated a transgene-dependent abnormal behavior likely due to the fact that it indirectly stimulates cortical-limbic glutamate output (McGrath *et al.*, 2000). Although a number of studies have looked at the acute effects of these drugs and their effect on glutamate release and the mGluR5 receptor, the result of chronic

administration on neurotransmitter and receptor level remains elusive. Therefore, it is of critical importance to have an understanding of the effect of these drugs in a healthy animal to assess and influence their ability to modify the glutamatergic system. Ketamine on the other hand has been used in a treatment setting in OCD before, with promising results (Bloch *et al.*, 2012; Rodriguez *et al.*, 2013). However, previous research has shown that the underlying working mechanisms of ketamine may be unique to ketamine and thus not be shared by all NMDA receptor antagonists (Hillhouse and Porter, 2014). Indeed, ketamine's mechanism of action remains mysterious, as besides its NMDA blockade, ketamine disturbs a wide range of intracellular neuronal processes (Sleigh *et al.*, 2014).

In this study we evaluated the potential of both MK-801 and Ebselen to modulate glutamate receptors and neurotransmitter levels in healthy naïve rats, by means of MRS, PET and IHC. This allowed us to investigate the effect on (i) the neurotransmitter level by visualisation of glumatate and glutamine with MRS, and (ii) on the neuroreceptor level, by visualising the receptor availability of mGluR5 and distribution by PET as well as to verify this with mGluR5 IHC. For future preclinical research, such adds to elucidating the role of glutamate in neuropathologies such as OCD, in particular in the QP model discussed earlier, to establish whether modifying the glutamate levels has an effect on the symptoms.

2. Methods

The present study was carried out in accordance with the European Communities Council Directive of November 24th, 1986 (86/609/EEC) for care of laboratory animals and after approval of the local ethical committee (University of Antwerp under number 2014-18). All efforts were made to minimize suffering and to reduce the number of animals. Naïve male Sprague Dawley rats (n=32; Harlan, the Netherlands, 285-550 g during the experiment) were housed in a temperature- and humidity-controlled vivarium in individually ventilated cages with a 12-hour light-dark cycle. All experiments were performed during daytime. Food and water were available ad libitum. All applicable institutional and national guidelines for the care and use of animals were followed.

2.1. Experimental Setup

Rats were divided into 3 groups. Animals of the first group (n = 12) received an intraperitoneal injection of MK-801 (0.3 mg/kg; dissolved in saline) every day at the same time (5:00-6:00 pm) for 7 consecutive days. This dosage was chosen based on previous work using MK-801 to induce glutamate toxicity (Kosten *et al.*, 2016) and an acute study investigating a variety of dosages (Wyckhuys *et al.*, 2013). Animals of the second group (n = 12) were exposed to Ebselen (10 mg/kg; dissolved in 0.5% carboxymethylcellulose) by oral gavage at the same time also for 7 consecutive days. The dosage of Ebselen was based on previous studies (Dalla Corte *et al.*, 2012; Yatmaz *et al.*, 2013; Ozyigit *et al.*, 2015; Oostwoud *et al.*, 2016). Animals of the third group (n = 8) received intraperitoneal injections of Saline (1 mL/kg) and served as a control.

A day after the 6th injection of either solution, to ensure that the drug was cleared from the brain, animals of each group were anaesthetised (induction of 5% isoflurane;

maintained at 2% isoflurane mixed with medical oxygen) and subjected to a PET/CT scan with ABP-688, performed on two dedicated small animal PET/CT scanners (Siemens Medical Solutions, Knoxville, TN; docked PET/CT and Siemens Inveon multimodal PET/CT) that have a reconstructed image resolution of approximately 1.2 mm at the centre of the field of view. PET data was acquired for a total of 60 minutes in list-mode format (frames: 2 x 10 s, 3 x 20 s, 3 x 30 s, 3 x 60 s, 3 x 150 s, and 9 x 300 s) with ABP-688 injected immediately after the start of the PET acquisition. After the PET scan, a CT image was acquired in three different bed positions. Small animal μPET-images were reconstructed by use of a 2D-OSEM with 4 iterations and 16 subsets after Fourier rebinning. The μPET images were then reconstructed on a 128 x 128 x 159 grid with a voxel size of 0.776 x 0.776 x 0.776 mm. Normalization, dead time correction, random subtraction, CT-based attenuation and single-scatter simulation corrections were applied (Watson, 2000).

The day after the 7th injection, animals underwent an MRS scan. All MR-based measurements were performed on a 7 Tesla Pharmascan (Avance III) with a horizontal bore (16 cm in diameter; Bruker Biospin, Ettlingen, Germany), equipped with a standard Bruker coil setup using a quadrature volume resonator for excitation and array rat head surface coil for signal detection. The system was interfaced to a Linux PC running Topspin 3.1 and Paravision 6.0.1 software (Bruker Biospin).

All rats were initially anesthetized using 5% isoflurane and maintained at 2% isoflurane in a mixture with medical oxygen. The volume of interest (VOI) for 1H-MRS was localized using multi-slice RARE images using a TurboRARE pulse sequence (Hennig *et al.*, 1986). A VOI (1.4 mm x 2.2 mm x 2.7 mm = 8.32 mm^3) was placed in the caudate putamen (CP) of the rat brain, as shown in figure 2a, by using the Paxinos and Watson rat brain atlas (6th edition) as a reference (between Bregma ± -0.24 mm and ± 1.92

mm). More details regarding this procedure can be found in the supplementary materials.

Following the MRS scan animals were sacrificed and their brains were removed and stored at -80 degrees Celsius. In order to verify the results of the PET scan, the brains of the animals of each group were subjected to a histological verification with an mGluR5 staining. In total, 8 animals of the Ebselen group were compared to 9 animals of the MK-801 group for the immunohistochemistry analysis, as one brain removal did not succeed.

2.2. PET analysis

Dynamic images were processed using PMOD 3.3 (PMOD Technologies, Zurich, Switzerland). After cropping, the static image corresponding to the time-averaged frames of each dynamic acquisition was spatially transformed to an in-house-developed rat brain template for ABP in a brain normalization step (Verhaeghe *et al.*, 2014). The obtained transformation was then applied to the dynamic image frames to equally transform those to the same ABP template. Extracerebral activity was removed by applying a brain mask available from the software. Time-activity curves (TAC's) of the investigated regions were extracted from the resulting dynamic images and used as the input for the Simplified Reference Tissue Model (SRTM) (Lammertsma and Hume, 1996), with the cerebellum (CB) as the reference. This kinetic modelling step subsequently produced the average binding potential (BPnd) of the Volume-of-Interest (VOI) of each region. Parametric BPnd maps were generated by pixelwise kinetic modelling using SRTM2. These BPnd output values were investigated by means of a VOI-based-analysis (with a predefined rat brain VOI template available in the software)

using a Mann-Whitney test, to compare the 2 conditions (MK-801 vs Ebselen) cross-sectionally. Additionally, a voxel-based analysis was performed using Statistical Parametric Mapping (SPM) on the aforementioned parametric BPnd maps. These data were analysed using an unpaired 2-sample t-test with a cluster-threshold of 125 voxels (1 mm^3) and a significance level of 0.01. The resulting T-maps were then again overlaid on the aforementioned brain VOI-template delineating the different brain regions displaying significant increases (hyper) in a red-yellow format and significant decreases (hypo) in a blue-green format.

2.3. MR analysis

In vivo 1H MR spectra were analysed using an automated deconvolution program (LCModel) (Provencher, 2001) as described previously (Orije *et al.*, 2015). The LCModel analysis was performed within the chemical shift range of 0.2 - 4.2 ppm. The following metabolites were included in the basis set of the LCModel (figure 2b): alanine, aspartate, creatine (Cr), phosphocreatine (PCr), γ-aminobutyric acid, glucose (Glc), glutamate (Glu), glutamine (Gln), glutathione (GSH), glycerophosphorylcholine (GPC), phosphorylcholine (PCh), Inositol (Ins), lactate, N-acetylaspartate (NAA), N-acetylaspartylglutamate (NAAG), scyllo-inositol and taurine (Tau). Besides this standard set of brain metabolites, LCModel includes 9 stimulated macromolecule and lipid peaks (Pfeuffer *et al.*, 1999) as shown in figure 2b. The results of macromolecules and lipds were not included in the study. The reliability of the metabolite quantification was assessed using the CRLB (estimated error of quantification) provided by the LCModel (Table 1).

Poorly fitted metabolite peaks (CRLB of >50%) were not included in further analysis. Metabolites with CRLB ≤ 50% in at least 50% of the spectra were included in the

neurochemical profile. Also, as neurometabolite levels fluctuate during the day, if the time of the MRS scan deviated from the originally foreseen time, this animal was not included in further analysis. This left us with a group size of 8 for the Ebselen group, a group size of 10 for the MK-801 group and a group size of 8 for the Control group. A group correlation matrix for metabolites was created. If the correlation between two metabolites was consistently high (i.e. correlation coefficient higher than -0.5), the sum of the metabolites was reported (Provencher, 2001). We computed a correlation matrix for metabolites quantified for all animals in order to assess which metabolites could be reliably resolved from each other. If the negative correlation between two metabolites was very strong (i.e. correlation coefficient higher than -0.6), it was considered that these two metabolites cannot be individually quantified (Provencher 2001). Therefore their sum was reported. The amplitudes of Cr and PCr were strongly correlated: the corresponding matrix element equals -0.9. The amplitudes of PCh and GPC were strongly correlated: the corresponding matrix element equals to -0.9. For these metabolites total creatine (tCr: Cr+ PCr) and total choline (tCho: GPC) were reported. Due to the higher field, Glu and Gln could be quantified individually with good accuracy. Absolute concentrations (in μmol/g) of metabolites were determined relative to an unsuppressed water signal acquired from the same VOI (Minati *et al.*, 2010). Further specifics on how these data were corrected can be found in supplementary. For the purpose of this paper we focused on the glutamate and glutamine levels and how these correlated with the other neurometabolites.

To estimate T2 maps of the CP, a rectangular ROI (± 0.05 cm^2) was manually defined for the left and right CP separately using the Paxinos and Watson rat brain atlas (6th edition) as a reference atlas. The data from left and right CP were averaged and recorded

as the T2 relaxation time. The coronal images acquired with MSME sequence for T2 mapping were analysed automatically with Paravision 6.01 as described previously, using the image sequence analysis tool (Kara *et al.*, 2015).

2.4. Immunohistochemistry

Coronal slices of the CP were made with a cryotome (Leica) at a thickness of 20 micrometres on Superfrost Plus slides (Thermo Scientific). These slices were stored at -80°C until staining. The staining procedure can be found in the supplementary materials.

All pictures were taken with an Nikon Ti wide-field microscope (Nikon Instuments, Paris, France), digitalized by Nikon Digital Sight DS-FI2 camera, using NIS Elements AR software, version 4.51.01 (Nikon Instruments).

Using Image J (Image J version 1.47) the mGluR5 receptor immunoreactivity was visualised. Analysis of the images consisted out of the evaluation of the the area fraction, which refers to the percentage of pixels in the image or selection that have been highlighted following a threshold, which was fixed at the same value for each image to eliminate any of the background.

3. Results and statistical analyses

Acute injection of MK-801 caused the animals of this group to display hyperactivity, consistent with what was previously described (Wu *et al.*, 2005). No other unexpected erratic behaviour was displayed over the course of the experiment. During the course of the scans, no aberrant behaviour was observed. Average weight of the animals receiving this drug at the start of the experiment was 326.42 ± 11.88 g. At the end of the experiment the average weight of these animals was significantly lower: 308.58 ± 9.93 g. Animals receiving Ebselen had an average weight of 331.33 ± 11.02 g at the beginning of the experiment, which significantly decreased to 322.17 ± 11.21 g at the end of the experiment. Animals of the control group had a weight of 353.96 ± 9.94 g at the scanning timepoint, that was significantly higher than the weight at the start of the experiment (324.80 ± 10 g).

3.1. PET Data

VOI-based analysis revealed a significant difference when comparing the BPnd in the CP between the Control animals (1.97 ± 0.39) and the animals receiving MK-801 (2.90 ± 0.47), constituting an increase of 47.21% ± 17.00%, or Ebselen (2.87 ± 0.46), constituting an increase of 45.69% ± 16.37% (figure 3).

This was confirmed with a voxel-based analysis ($p = 0.01$, cluster size = 125 voxels) investigating all regions using SPM, displaying strong significant ($p < 0.01$) increases after either drug in the frontal regions of the brain, in particular the majority of the CP, the cortex, hippocampus and amygdala. Furthermore there were significant ($p < 0.01$) decreases in the majority of the CB (figure 4).

3.2. Immunohistochemistry

Analysis revealed a significant ($p < 0.05$) difference on area percentage in the CP between control and ebselen, with an area fraction of 60.83% ± 6.30% for Ebselen and 50.21% ± 5.71% for Saline (figure 5). MK-801 had an area fraction of 57.14% ± 9.23%, not significantly different but with a tendency to increase.

3.3. MRS Data

No significant changes were found on glutamate level when comparing chronic Ebselen and chronic MK-801 to Control. However, a significant difference ($p < 0.05$) between the Ebselen and Control animals was found in the levels of glutamine. Animals treated with Ebselen had a mean glutamine concentration of 2.2 ± 0.4 μmol/g, which was 18.52% ± 5.42% lower than animals of the Control group having a mean of 2.7 ± 0.3 μmol/g. Animals of the MK-801 group had a mean of 2.9 ± 0.5 μmol/g which was 7.41% ± 2.10% higher than the Control animals. Also, when considering the ratio of glutamate vs glutamaine, a significant difference ($p < 0.01$) was present between the Ebselen and Control group with a mean of 4.1 ± 0.6 for Ebselen, 32.26% ± 8.88% higher than the ratio for the Control animals (3.1 ± 0.4; figure 6). This ratio was correlated ($p <0.05$) with glutamine but not with glutamate.

A correlation between the MRS signal and the BPnd of the CP revealed no significant correlation with any of the neurometabolites ($p > 0.05$).

The mean T2 values of the CP of the rats receiving Ebselen and MK-801 were not statistically significant from the rats receiving Control ($p < 0.05$, two tailed student's test n = 8 for each group). The values were estimated as 40.76 ± 0.74 ms, 40.95 ± 0.80 ms and 41.255 ± 0.68 for the MK-801, Ebselen and Control exposed groups respectively.

4. Discussion

This study evaluated the potential of both Ebselen and MK-801 to affect the glutamate receptors and neurotransmitter levels in healthy naïve rats, as possible modulators for the preclinical QP induced OCD model. Previous work established that Ebselen has a direct effect on the glutamatergic system, by reducing the K^+-evoked release of glutamate (Nogueira *et al.*, 2002; Moretto *et al.*, 2007) while low dosages of MK-801 selectively block NMDARs in the GABAergic interneurons, thus increasing glutamate release (Xi *et al.*, 2009). A previous study performed by our lab confirmed glutamate increases when MK-801 was given acutely. Other NMDA antagonists, such as ketamine, when administered acutely, also increase glutamate (Wyckhuys *et al.*, 2013). Contrarily, MK-801 appears to decrease glutamate levels when administered chronically, which is potentially caused by chronic blockade of the NMDA receptor, making non-NMDA Glu receptors discompensatory and decrease the terminal excitability of glutamateric neurons, resulting in an attenuation of the Glu levels (Tsukada *et al.*, 2005; Zuo *et al.*, 2006). Alternatively, this decrease of Glu might also be caused by postsynaptic inhibition of other neuronal systems to NMDA receptor-mediated neurotransmission (Tsukada *et al.*, 2005; Zuo *et al.*, 2006). Another explanation can be found in the up-regulation of Glu transporters (Tsukada *et al.*, 2005; Zuo *et al.*, 2006).

After chronic Ebselen the increase in mGluR5 area fraction measured by IHC was significant, indicating more mGluR5 distribution possibly as a result of chronically less endogenous glutamate. For MK-801 a similar trend is noticeable, albeit not significant with the current power.

Also the PET/CT results showed significant increases in BPnd after chronic administration of both Ebselen and MK-801 also indicating more availability of the

mGluR5 receptor. MK-801 is not the only NMDA-antagonist that was investigated by ABP688. Previously a clinical study used this tracer to investigate the acute effect of ketamine (0.23 mg/kg over 1 min, then 0.58 mg/kg over 1h), with the intention of increasing Glu, and reported significant decreases in BPnd. As ABP688 binds at different sites on the receptor and hence does not compete with glutamate, one could at first sight hypothesise that glutamate fluctuations do not influence the BPnd. However, it should be noted that the affinity of the receptor for the tracer is in part determined by the endogenous glutamate. For example, DeLorenzo et al. used N-acetylcysteine, which is known to increase extracellular glutamate, and reported decreases in BPnd (Delorenzo *et al.*, 2015). Similarly, Zimmer et al. used ceftriaxone to decrease extracellular levels of glutamate and reported increases in the BPnd of ABP688 (Zimmer *et al.*, 2015). Therefore, our results, displaying strong increases in BPnd after treatment with Ebselen or MK-801, when compared to Control, indicate lower levels of extracellular glutamate that are positively affecting affinity of the tracer for mGluR5 consistent with previous data (Tsukada *et al.*, 2005; Zuo *et al.*, 2006). It is thus possible that there is an overestimation of the increase in mGluR5 distribution in the PET/CT results, due to the increase in tracer affinity caused by a decrease in extracellular glutamate. Alternatively, as NMDA and mGluR5 are interconnected in the brain, it is plausible for the changes induced by MK-801 only to be present on the level of receptor interaction and not on glutamate release.

In contrast to the results from the PET/CT and immunohistochemistry, indicating decreased levels of glutamate, the MRS scan showed that the chronic exposure to either drug, did not affect glutamate levels in such a way that it differed from the Control condition in the visualised time frame. When considering the PET/CT and

immunohistochemistry results, this seems to contradict the hypothesis of a decrease in glutamate. However, it is important to note that MRS visualizes the total glutamate pool as it does not discriminate between intracellular and extracellular neurochemicals. The concentration of the neurochemicals is mostly driven by the intracellular concentration, due to the negligible volume of the extracellular space. It could thus be that the release of glutamate in the extracellular space is in fact changed, directly affecting the glutamate receptors as visualized by PET/CT and immunohistochemistry. Interestingly, when considering this flux of Glu and Gln, there were significant decreases in Gln after chronic injection with Ebselen. Because animals are repeatedly exposure to the drug, certain compensatory changes could occur. As glutamate is readily converted into glutamine, through the glutamine synthetase pathway by astrocytes, it could be that due to decreased glutamate levels after chronic administration of Ebselen, the available glutamine was converted into glutamate to preserve a normal level of glutamate, thereby depleting the Gln pool to compensate for this as the acute effect of Ebselen wears off. As the amount of glutamate present in the synapse is maintained homeostatically at a low level at all times, with 85% of glutamate being converted to glutamine (Hertz, 2013) and Ebselen acutely decreasing Glu levels, this could explain the distorted balance in Glu/Gln ratio after administration of Ebselen. Although this ratio had a tendency to increase after chronic administration of MK-801, this was not significant in this particular group.

In conclusion, both Ebselen and MK-801 affect the mGluR5 receptor when administered chronically in the dosages described in this study. Although no direct effects on total glutamate were visualized with MRS, the changes in glutamine do hint towards changes in the total Glu-Gln pool.

Taken together, these two drugs are interesting modulators for further investigation in glutamatergic pathologies such as obsessive compulsive disorder, fragile x, epilepsy and autism, and for further elucidation of their working mechanisms in order to optimize their use and potential.

5. Acknowledgements

This work was funded by Antwerp University, Belgium through a PhD grant for S. Servaes and D. Glorie, an assistant professor position for J. Verhaeghe, a full professor position for S. Staelens and S. Stroobants. S. Stroobants is also supported by Antwerp University Hospital, Belgium through a departmental position. Firat Kara is a holder of an FWO-Vlaanderen (Belgium) post-doctoral fellowship (postdoctoral FWO number: 12S4815N). Hardware and experimental costs were supported by a DOCPRO (41/FA020000/FFB140317) and an FWO KAN (42/FA020000/685) of Antwerp University. No funding sources had a role in the study design or in the collection, analysis and interpretation of the data.

The authors would like to thank Philippe Joye, Caroline Berghmans and Annemie Van Eetveldt for their expertise and technical assistance.

6. Authorship Contributions

Participated in research design: S. Servaes, F. Kara, D. Glorie, S. Staelens

Conducted experiments: S. Servaes, F. Kara

Performed data analysis: S. Servaes, F. Kara

Wrote or contributed to the writing of the manuscript: S. Servaes, F. Kara, A. Van Der Linden, S. Stroobants, S. Staelens

References

Ade KK, Wan Y, Hamann HC, O'Hare JK, Guo W, Quian A, Kumar S, Bhagat S, Rodriguiz RM, Wetsel WC, Conn PJ, Dzirasa K, Huber KM, and Calakos N (2016) Increased Metabotropic Glutamate Receptor 5 Signaling Underlies Obsessive-Compulsive Disorder-like Behavioral and Striatal Circuit Abnormalities in Mice. *Biol Psychiatry* **80**:522–533.

Albelda N, Bar-On N, and Joel D (2010) The role of NMDA receptors in the signal attenuation rat model of obsessive-compulsive disorder. *Psychopharmacology (Berl)* **210**:13–24.

Arnold P, Rosenberg D, Mundo E, Tharmalingam S, Kennedy J, and Richter M (2004) Association of a glutamate (NMDA) subunit receptor gene (GRIN2B) with obsessive-compulsive disorder: a preliminary study. *Psychopharmacology (Berl)* **174**.

Azad GK, and Tomar RS (2014) Ebselen, a promising antioxidant drug: Mechanisms of action and targets of biological pathways.

Bloch MH, Wasylink S, Landeros-Weisenberger A, Panza KE, Billingslea E, Leckman JF, Krystal JH, Bhagwagar Z, Sanacora G, and Pittenger C (2012) Effects of ketamine in treatment-refractory obsessive-compulsive disorder. *Biol Psychiatry*, doi: 10.1016/j.biopsych.2012.05.028.

Chakrabarty K, Bhattacharyya S, Christopher R, and Khanna S (2005) Glutamatergic dysfunction in OCD. *Neuropsychopharmacology* **30**:1735–40.

Chana G, Laskaris L, Pantelis C, Gillett P, Testa R, Zantomio D, Burrows EL, Hannan AJ, Everall IP, and Skafidas E (2015) Decreased expression of mGluR5

within the dorsolateral prefrontal cortex in autism and increased microglial number in mGluR5 knockout mice: Pathophysiological and neurobehavioral implications. *Brain Behav Immun*, doi: 10.1016/j.bbi.2015.05.009.

Coyle JT (2006) Glutamate and Schizophrenia: Beyond the Dopamine Hypothesis. *Cell Mol Neurobiol* **26**:4–6.

Dalla Corte CL, Bastos LL, Dobrachinski F, Rocha JBT, and Soares FAA (2012) The combination of organoselenium compounds and guanosine prevents glutamate-induced oxidative stress in different regions of rat brains. *Brain Res* **1430**:101–111.

Delorenzo C, Dellagioia N, Bloch M, Sanacora G, Nabulsi N, Abdallah C, Yang J, Wen R, Mann JJ, Krystal JH, Parsey R V., Carson RE, and Esterlis I (2015) In vivo ketamine-induced changes in [11C]ABP688 binding to metabotropic glutamate receptor subtype 5. *Biol Psychiatry* **77**:266–275.

Denys D, Mantione M, Figee M, van den Munckhof P, Koerselman F, Westenberg H, Bosch A, and Schuurman R (2010) Deep Brain Stimulation of the Nucleus Accumbens for Treatment-Refractory Obsessive-Compulsive Disorder. *Arch Gen Psychiatry* **67**:1061.

Ghasemi M, and Schachter SC (2011) The NMDA receptor complex as a therapeutic target in epilepsy: A review.

Hennig J, Nauerth A, and Friedburg H (1986) RARE imaging: A fast imaging method for clinical MR. *Magn Reson Med* **3**:823–833.

Hertz L (2013) The glutamate-glutamine (GABA) cycle: Importance of late postnatal

development and potential reciprocal interactions between biosynthesis and degradation. *Front Endocrinol (Lausanne)* **4**:1–16.

Hillhouse TM, and Porter JH (2014) Ketamine, but not MK-801, produces antidepressant-like effects in rats responding on a differential-reinforcement-of-low-rate operant schedule. *Behav Pharmacol*, doi: 10.1097/FBP.0000000000000014.

Kara F, Höfling C, Roßner S, Schliebs R, Van der Linden A, Groot HJM, and Alia A (2015) In Vivo Longitudinal Monitoring of Changes in the Corpus Callosum Integrity During Disease Progression in a Mouse Model of Alzheimer's Disease. *Curr Alzheimer Res* **12**:941–50.

Kelly E, Schaeffer SM, Dhamne SC, Lipton JO, Lindemann L, Honer M, Jaeschke G, Super CE, Lammers SH, Modi ME, Silverman JL, Dreier JR, Kwiatkowski DJ, Rotenberg A, and Sahin M (2018) MGluR5 Modulation of Behavioral and Epileptic Phenotypes in a Mouse Model of Tuberous Sclerosis Complex. *Neuropsychopharmacology*, doi: 10.1038/npp.2017.295.

Kosten L, Verhaeghe J, Verkerk R, Thomae D, De Picker L, wyffels L, Van Eetveldt A, Dedeurwaerdere S, Stroobants S, and Staelens S (2016) Multiprobe molecular imaging of an NMDA receptor hypofunction rat model for glutamatergic dysfunction. *Psychiatry Res - Neuroimaging* **248**:1–11.

Lammertsma AA, and Hume SP (1996) Simplified reference tissue model for PET receptor studies. *Neuroimage* **4**:153–8.

Lee E-J, Choi SY, and Kim E (2015) NMDA receptor dysfunction in autism spectrum disorders. *Curr Opin Pharmacol*, doi: 10.1016/j.coph.2014.10.007.

McGrath MJ, Campbell KM, Parks CR, and Burton FH (2000) Glutamatergic drugs exacerbate symptomatic behavior in a transgenic model of comorbid Tourette's syndrome and obsessive-compulsive disorder. *Brain Res*, doi: 10.1016/S0006-8993(00)02646-9.

Meldrum BS (2000) Glutamate as a neurotransmitter in the brain: review of physiology and pathology. *J Nutr* **130**:1007S–15S.

Miladinovic T, Nashed MG, and Singh G (2015) Overview of glutamatergic dysregulation in central pathologies.

Minati L, Aquino D, Bruzzone MG, and Erbetta A (2010) Quantitation of normal metabolite concentrations in six brain regions by in-vivoH-MR spectroscopy. *J Med Phys* **35**:154–163.

Moretto MB, Thomazi AP, Godinho G, Roessler TM, Nogueira CW, Souza DO, Wofchuk S, and Rocha JBT (2007) Ebselen and diorganylchalcogenides decrease in vitro glutamate uptake by RAT brain slices: Prevention by DTT and GSH. *Toxicol Vitr* **21**:639–645.

Nogueira CW, Rotta LN, Zeni G, Souza DO, and Rocha JBT (2002) Exposure to ebselen changes glutamate uptake and release by rat brain synaptosomes. *Neurochem Res* **27**:283–8.

Oostwoud LC, Gunasinghe P, Seow HJ, Ye JM, Selemidis S, Bozinovski S, and Vlahos R (2016) Apocynin and ebselen reduce influenza A virus-induced lung inflammation in cigarette smoke-exposed mice. *Sci Rep*, doi: 10.1038/srep20983.

Orije J, Kara F, Guglielmetti C, Praet J, Van der Linden A, Ponsaerts P, and Verhoye

M (2015) Longitudinal monitoring of metabolic alterations in cuprizone mouse model of multiple sclerosis using 1H-magnetic resonance spectroscopy. *Neuroimage* **114**:128–135.

Ozyigit F, Kucuk A, Akcer S, Tosun M, Kocak FE, Kocak C, Kocak A, Metineren H, and Genc O (2015) Different dose-dependent effects of ebselen in sciatic nerve ischemia-reperfusion injury in rats. *Bosn J Basic Med Sci*, doi: 10.17305/bjbms.2015.521.

Pfeuffer J, Tkáč I, Provencher SW, and Gruetter R (1999) Toward an in Vivo Neurochemical Profile: Quantification of 18 Metabolites in Short-Echo-Time 1H NMR Spectra of the Rat Brain. *J Magn Reson* **141**:104–120.

Pittenger C, Bloch MH, and Williams K (2011) Glutamate abnormalities in obsessive compulsive disorder: Neurobiology, pathophysiology, and treatment. *Pharmacol Ther* **132**:314–332.

Pop AS, Gomez-Mancilla B, Neri G, Willemsen R, and Gasparini F (2014) Fragile X syndrome: A preclinical review on metabotropic glutamate receptor 5 (mGluR5) antagonists and drug development.

Porciúncula LO, Rocha JBT, Boeck CR, Vendite D, and Souza DO (2001) Ebselen prevents excitotoxicity provoked by glutamate in rat cerebellar granule neurons. *Neurosci Lett* **299**:217–220.

Provencher SW (2001) Automatic quantitation of localized in vivo 1H spectra with LCModel. *NMR Biomed* **14**:260–264.

Rodriguez CI, Kegeles LS, Levinson A, Feng T, Marcus SM, Vermes D, Flood P, and

Simpson HB (2013) Randomized controlled crossover trial of ketamine in obsessive-compulsive disorder: proof-of-concept. *Neuropsychopharmacology*, doi: 10.1038/npp.2013.150.

Schewe T (1995) Molecular actions of Ebselen-an antiinflammatory antioxidant.

Seo JY, Lee CH, Cho JH, Choi JH, Yoo KY, Kim DW, Park OK, Li H, Choi SY, Hwang IK, and Won MH (2009) Neuroprotection of ebselen against ischemia/reperfusion injury involves GABA shunt enzymes. *J Neurol Sci* **285**:88–94.

Servaes S, Glorie D, Verhaeghe J, Stroobants S, and Staelens S (2017) Preclinical molecular imaging of glutamatergic and dopaminergic neuroreceptor kinetics in obsessive compulsive disorder. *Prog Neuro-Psychopharmacology Biol Psychiatry* **77**:90–98.

Shannon HE, and Love PL (2004) Within-session repeated acquisition behavior in rats as a potential model of executive function. *Eur J Pharmacol*, doi: 10.1016/j.ejphar.2004.04.054.

Sleigh J, Harvey M, Voss L, and Denny B (2014) Ketamine - more mechanisms of action than just NMDA blockade.

Thomas AG, Rojas C, Tanega C, Shen M, Simeonov A, Boxer MB, Auld DS, Ferraris D V., Tsukamoto T, and Slusher BS (2013) Kinetic characterization of ebselen, chelerythrine and apomorphine as glutaminase inhibitors. *Biochem Biophys Res Commun* **438**:243–248.

Tsukada H, Nishiyama S, Fukumoto D, Sato K, Kakiuchi T, and Domino EF (2005)

Chronic NMDA antagonism impairs working memory, decreases extracellular dopamine, and increases D1receptor binding in prefrontal cortex of conscious monkeys. *Neuropsychopharmacology* **30**:1861–1869.

Verhaeghe J, Wyffels L, Wyckhuys T, Stroobants S, and Staelens S (2014) Rat brain normalization templates for robust regional analysis of [11C]ABP688 positron emission tomography/computed tomography. TL - 13. *Mol Imaging* **13 VN-r**:1–14.

Watson CC (2000) New, faster, image-based scatter correction for 3D PET. *IEEE Trans Nucl Sci* **47**:1587–1594.

Welch JM, Lu J, Rodriguiz RM, Trotta NC, Peca J, Ding J-D, Feliciano C, Chen M, Adams JP, Luo J, Dudek SM, Weinberg RJ, Calakos N, Wetsel WC, and Feng G (2007) Cortico-striatal synaptic defects and OCD-like behaviours in Sapap3-mutant mice. *Nature* **448**:894–900.

Wu J, Zou H, Strong JA, Yu J, Zhou X, Xie Q, Zhao G, Jin M, and Yu L (2005) Bimodal effects of MK-801 on locomotion and stereotypy in C57BL/6 mice. *Psychopharmacology (Berl)* **177**:256–263.

Wyckhuys T, Verhaeghe J, Wyffels L, Langlois X, Schmidt M, Stroobants S, and Staelens S (2013) N-Acetylcysteine– and MK-801–Induced Changes in Glutamate Levels Do Not Affect In Vivo Binding of Metabotropic Glutamate 5 Receptor Radioligand 11 C-ABP688 in Rat Brain. *J Nucl Med* **54**:1–8.

Xi D, Zhang W, Wang H-X, Stradtman Iii GG, Gao W-J, and Gao W-J (2009) Dizocilpine (MK-801) induces distinct changes of N-methyl-D- aspartic acid receptor subunits in parvalbumin-containing interneurons in young adult rat

prefrontal cortex. *Int J Neuropsychopharmacol* **12**:1395–1408.

Yatmaz S, Seow HJ, Gualano RC, Wong ZX, Stambas J, Selemidis S, Crack PJ, Bozinovski S, Anderson GP, and Vlahos R (2013) Glutathione peroxidase-1 reduces influenza A virus-induced lung inflammation. *Am J Respir Cell Mol Biol*, doi: 10.1165/rcmb.2011-0345OC.

Zimmer ER, Parent MJ, Leuzy A, Aliaga A, Aliaga A, Moquin L, Schirrmacher ES, Soucy J-P, Skelin I, Gratton A, Gauthier S, and Rosa-Neto P (2015) Imaging in vivo glutamate fluctuations with [11C]ABP688: a GLT-1 challenge with ceftriaxone. *J Cereb Blood Flow Metab* 1–6.

Zuo DY, Zhang YH, Cao Y, Wu CF, Tanaka M, and Wu YL (2006) Effect of acute and chronic MK-801 administration on extracellular glutamate and ascorbic acid release in the prefrontal cortex of freely moving mice on line with open-field behavior. *Life Sci* **78**:2172–2178.

Footnotes

Financial Support:

This work was supported by a DocPro from the University of Antwerp [41/FA020000/FFB140317] and the Fonds Wetenschappelijk Onderzoek from the University of Antwerp [42/FA020000/685].

Figure Legends

Figure 1

The frontal cortex, responsible for functions such as error detection, working memory and goal-directed behaviour sends signals through the striatum through glutamatergic afferents. From the striatum, this signal either inhibits or reduces the inhibition to the thalamus, dependent on the levels of DA present. From the thalamus a signal is sent back to the frontal cortex, completing a feedback loop. It has been hypothesised that OCD results from a dysfunction in this circuit, in particular in the downstream signalling pathway. As the brain is exposed to higher levels of glutamate, this will likely cause overstimulation and disruption of the circuits and receptors in place.

Figure 2

A) The VOI is positioned at the caudate putamen (indicated by the red boxes on T2 weighted axial and coronal images).

B) The major peaks are labelled on the representative spectra. Ins: inositol; tCho: PCho+ GPC; Tau: taurine; tCr: PCr+Cr; Gln: glutamine; Glu: glutamate, Lac: Lactate. The voxel size is 8.32 mm^3.

Figure 3

A) BPnd maps of ABP-688 for both Ebselen (top) and MK-801 (middle) and Saline (bottom) are displayed, with higher values displayed in red and lower values in a green-blue format.

B) BPnd values plotted showing the difference between the different groups.

Figure 4

SPM maps of ABP-688 for both Ebselen (A) and MK-801 (B) vs Saline with significant higher t-values (hyper metabolism) displayed in red and significant lower t-values (hypo metabolism) in a blue-green format.

Figure 5

A: Overview image of the CP after immunohistochemistry (20x) with the mGluR5 antibody. Arrows point to cells with densily stained membranes rich in mGluR5.

B: Investigated parameter of the immunohistochemistry is presented here (Area percentage) after chronic Ebselen (n = 8) chronic MK-801 (n = 9) and Saline (n = 8). Individual points, median and standard deviation of each group are displayed.

C: Overview images of the three different conditions (left to right: ebselen, MK-801, Saline)

* $p < 0.05$

Figure 6

The investigated MRS parameters (Glutamate, Glutamine and the ratio between the two) extracted from the MRS spectrum are plotted here for both Ebselen (n = 8) and MK-801 (n = 10). Individual points, median and standard deviation of the group are displayed. * $p < 0.05$; ** $p < 0.01$

JPET Fast Forward. Published on December 14, 2018 as DOI: 10.1124/jpet.118.252635
This article has not been copyedited and formatted. The final version may differ from this version.

Tables

Table 1: Metabolite concentrations (in μmol/g) and CRLB values

Metabolite	concentration (μmol/g) mean ± SD			CRLB-Control	CRLB-Ebselen	CRLB-MK-801
	Control (n=8)	Ebselen (n=8)	MK-801 (n=10)			
tCr	6.1 ± 0.5	6.1 ± 0.3	6.0 ± 0.5	6%	6%	6%
GABA	1.3 ± 0.3	1.5 ± 0.2	1.4 ± 0.4	29%	24%	26%
Glc	1.3 ± 0.5	1.3 ± 0.3	1.4 ± 0.2	38%	35%	31%
Gln	2.7 ± 0.3	2.2 ± 0.4	2.9 ± 0.5	18%	22%	18%
Glu	8.4 ± 0.7	8.9 ± 1.1	8.8 ± 0.3	6%	6%	6%
tCh	1.3 ± 0.1	1.4 ± 0.2	1.4 ± 0.1	9%	8%	8%
GSH	1.1 ± 0.2	1.3 ± 0.5	1.4 ± 0.4	24%	22%	21%
Ins	2.9 ± 0.5	2.7 ± 0.7	2.5 ± 0.6	14%	16%	17%
Lac	1.3 ± 0.5	1.5 ± 0.7	1.4 ± 0.3	32%	31%	31%
NAA	6.7 ± 0.4	6.4 ± 0.4	6.2 ± 0.5	6%	6%	6%
Tau	9.0 ± 0.5	7.9 ± 0.6	8.3 ± 0.7	5%	6%	6%

JPET Fast Forward. Published on December 14, 2018 as DOI: 10.1124/jpet.118.252635
This article has not been copyedited and formatted. The final version may differ from this version.

Figures

Figure 1

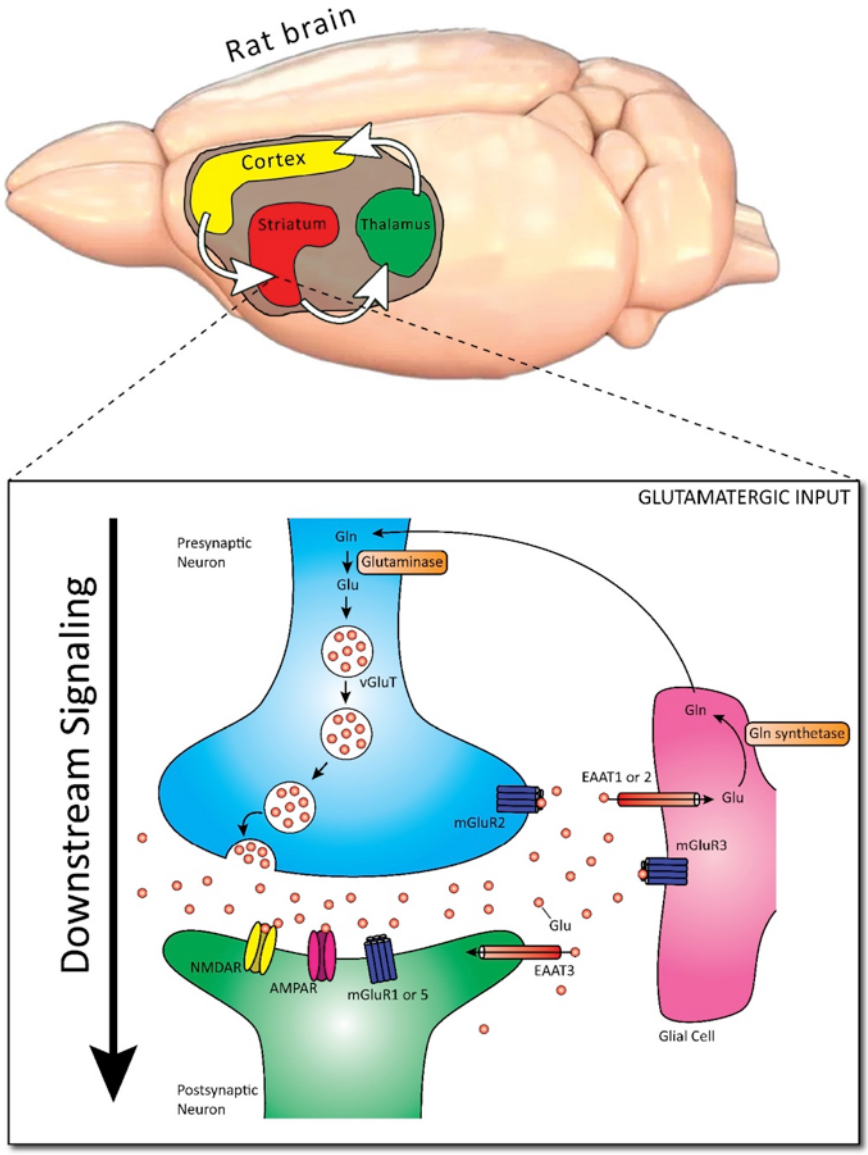

JPET Fast Forward. Published on December 14, 2018 as DOI: 10.1124/jpet.118.252635
This article has not been copyedited and formatted. The final version may differ from this version.

Figure 2

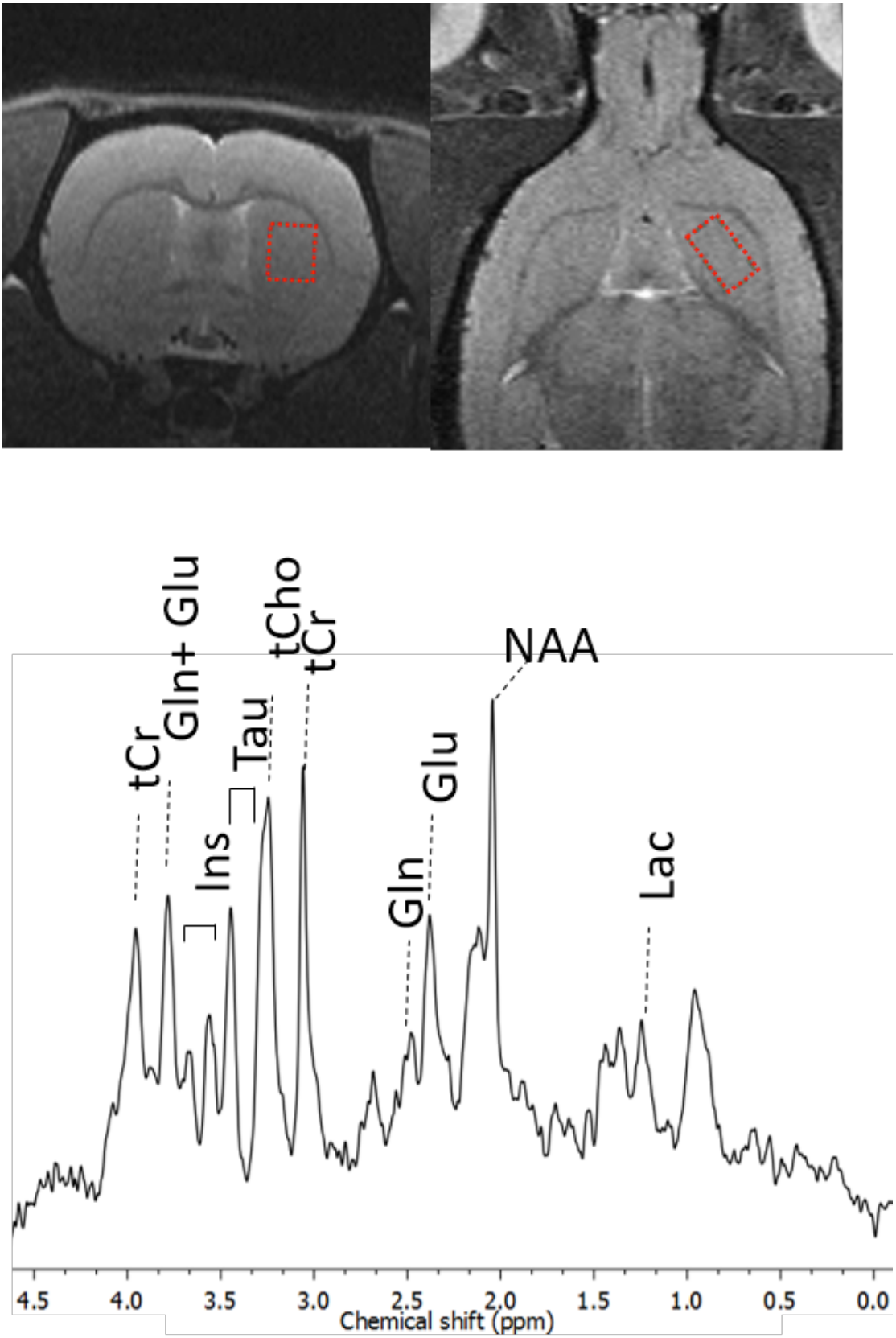

JPET Fast Forward. Published on December 14, 2018 as DOI: 10.1124/jpet.118.252635
This article has not been copyedited and formatted. The final version may differ from this version.

Figure 3

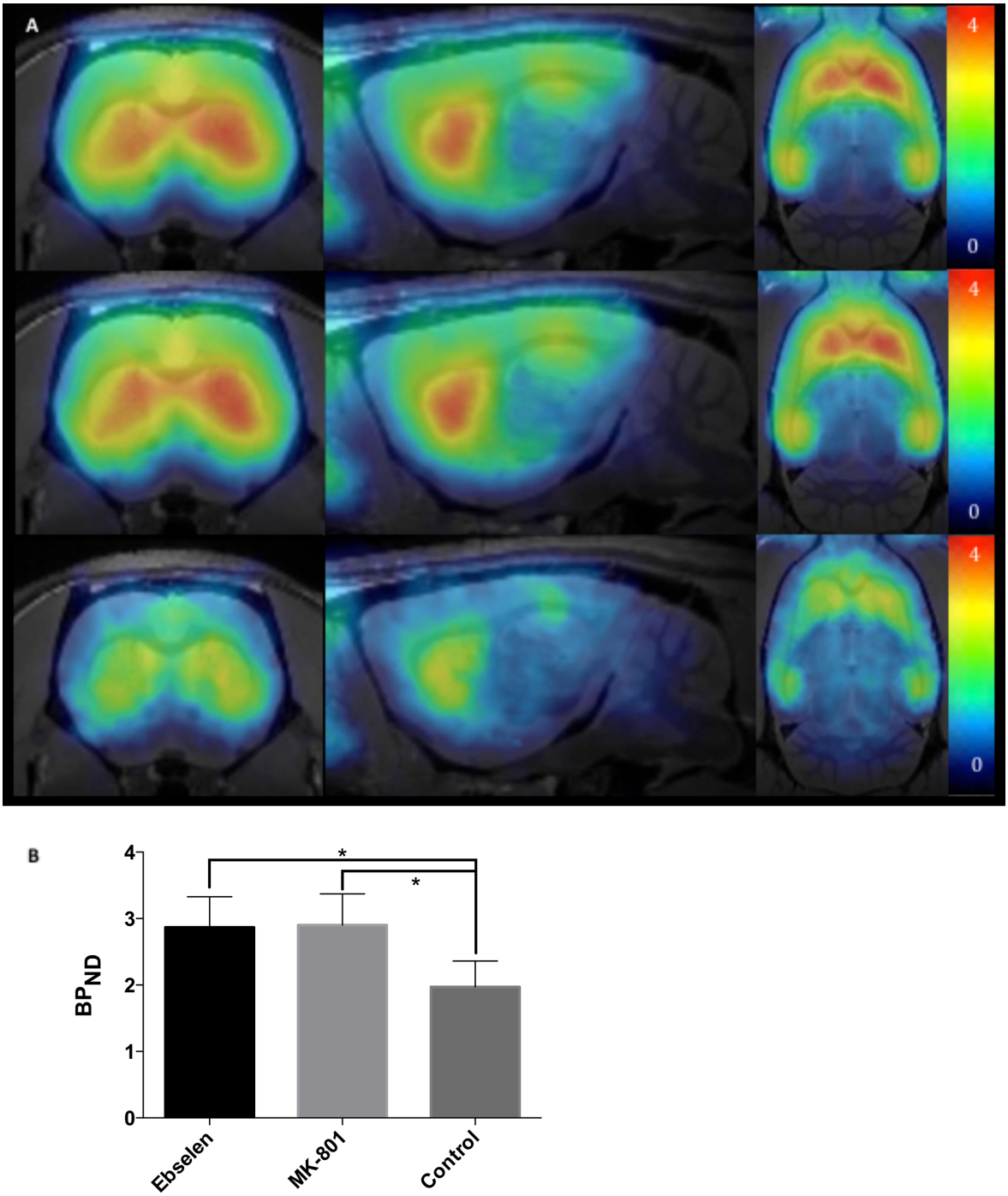

JPET Fast Forward. Published on December 14, 2018 as DOI: 10.1124/jpet.118.252635
This article has not been copyedited and formatted. The final version may differ from this version.

Figure 4

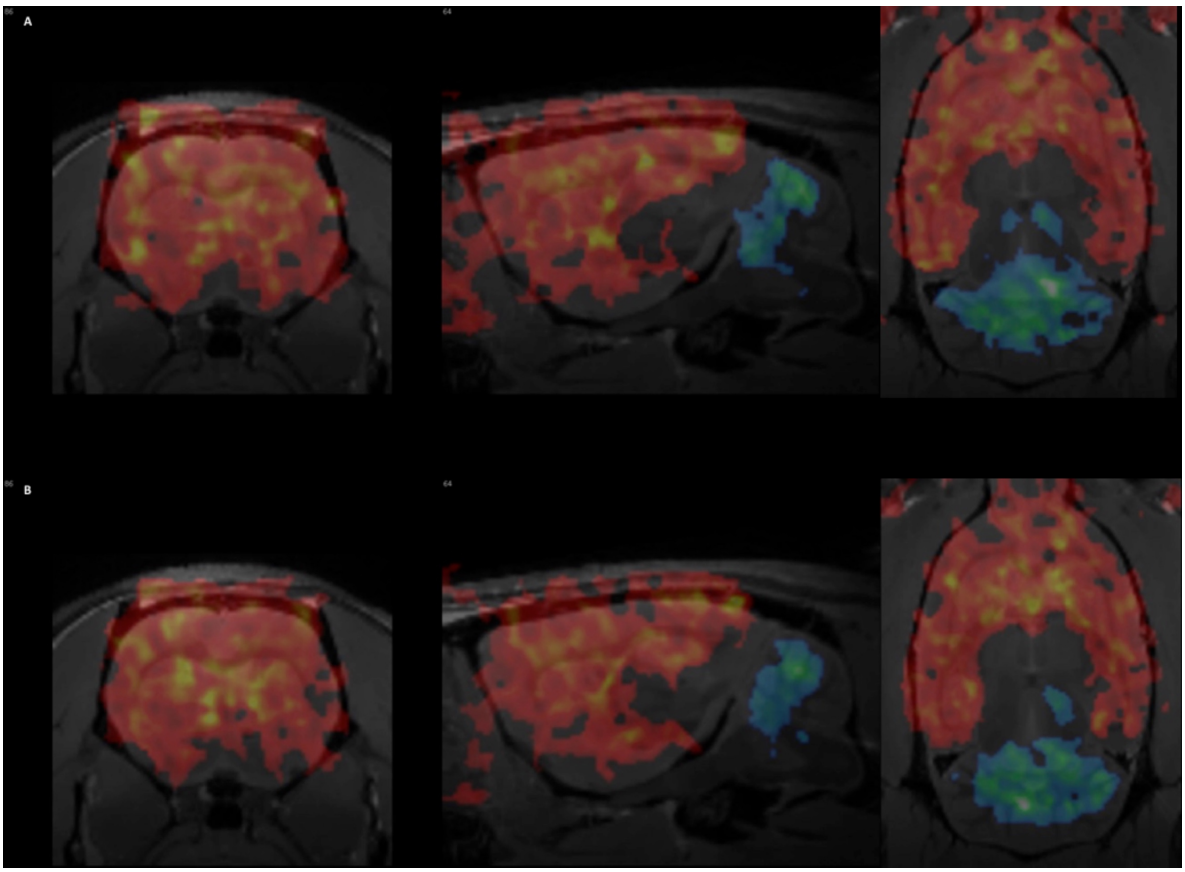

JPET Fast Forward. Published on December 14, 2018 as DOI: 10.1124/jpet.118.252635
This article has not been copyedited and formatted. The final version may differ from this version.

Figure 5

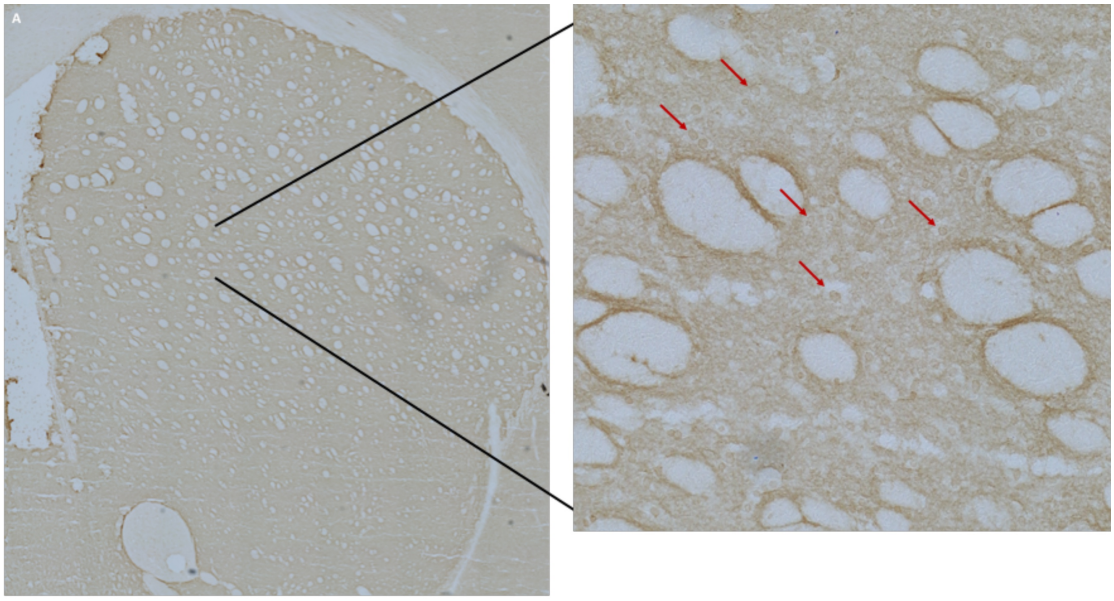

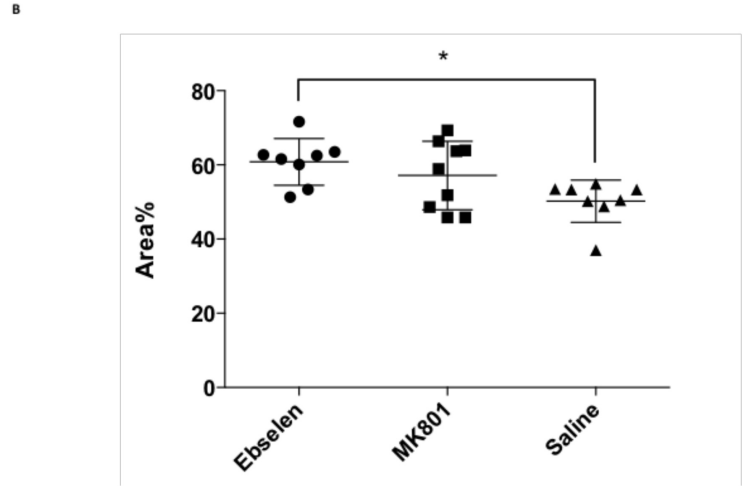

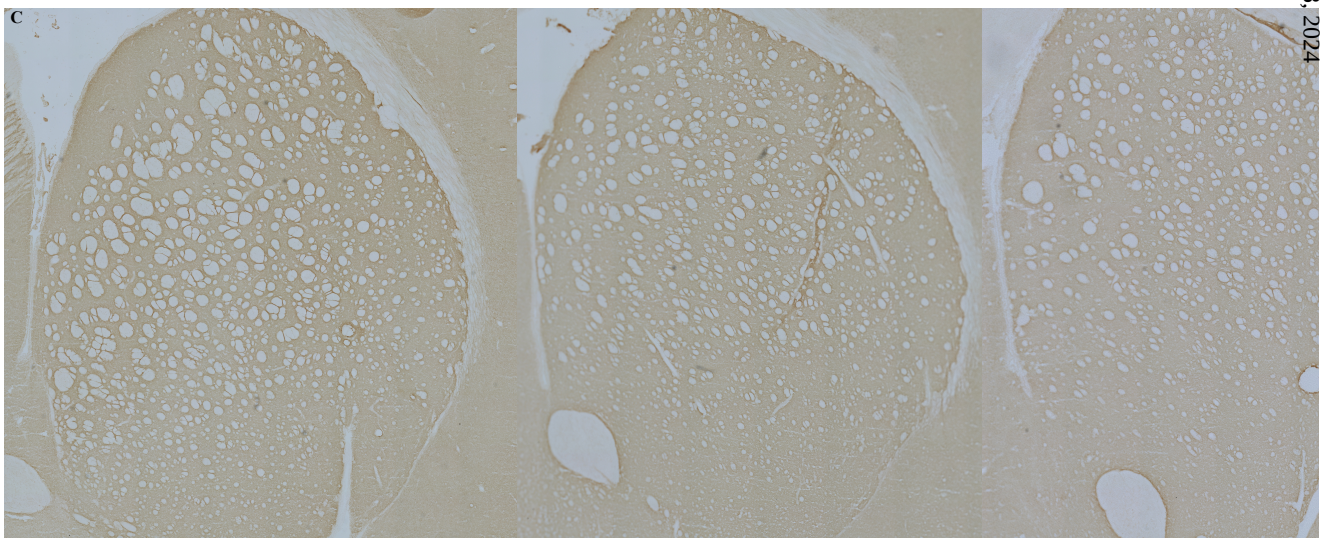

JPET Fast Forward. Published on December 14, 2018 as DOI: 10.1124/jpet.118.252635
This article has not been copyedited and formatted. The final version may differ from this version.

JPET Fast Forward. Published on December 14, 2018 as DOI: 10.1124/jpet.118.252635
This article has not been copyedited and formatted. The final version may differ from this version.

Figure 6

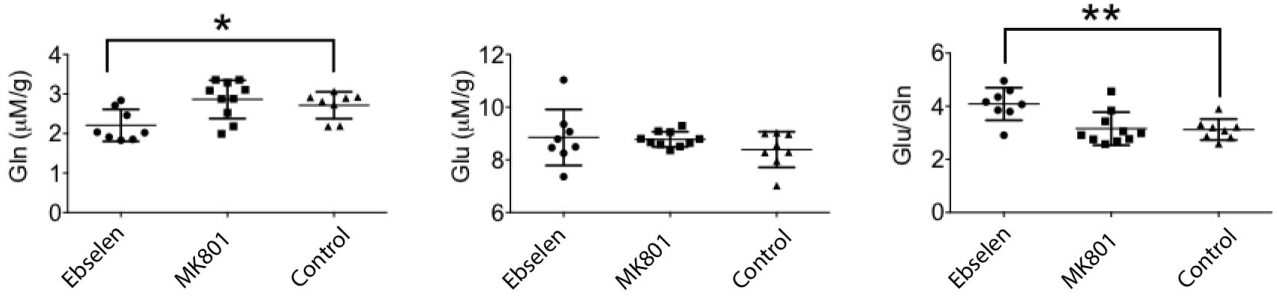

SUPPLEMENTARY TO: IN VIVO PRECLINICAL MOLECULAR IMAGING OF REPEATED EXPOSURE TO AN NMDA ANTAGONIST AND A GLUTAMINASE INHIBITOR AS POTENTIAL GLUTAMATERGIC MODULATORS.

Stijn Servaes[1], Firat Kara[2], Dorien Glorie[1], Sigrid Stroobants[1,3], Annemie Van Der Linden[2], Steven Staelens[1,*]

---

[1] *Molecular Imaging Center Antwerp (MICA), University of Antwerp, Universiteitsplein 1, 2610, Wilrijk, Antwerp, BELGIUM*

[2] *Bio-Imaging Lab (BIL), University of Antwerp, Universiteitsplein 1, 2610, Wilrijk, Antwerp, BELGIUM*

[3] *Department of Nuclear Medicine, University Hospital Antwerp, Wilrijkstraat 10, 2650, Edegem, Antwerp, BELGIUM*

1. PET acquisition

Throughout the experiment, respiration rates were visually monitored. Body temperature of the animals was maintained by using a heated pad.

The PET data were reconstructed both into a single static image of the full 60 minutes and into 33 temporal bins of increasing duration (12 × 10, 3 × 20, 3 × 30, 3 × 60, 3 × 150, and 9 × 300 seconds) using a two-dimensional ordered subset expectation maximization (2D-OSEM) with 4 iterations and 16 subsets after Fourier rebinning. The μPET images were then reconstructed on a 128x128x159 grid with a voxel size of 0.776 x 0.776 x 0.796 mm. Normalization, dead time correction, random subtraction, CT-based attenuation and single-scatter simulation corrections were applied (Watson, 2000).

2. MR acquisition

Throughout the MR studies, respiration rate was constantly monitored by a pressure sensitive respiration sensor, placed under the abdomen. Body temperature was monitored with a rectal temperature probe and was maintained at 37.0 ± 0.5°C using a warm air system with a feedback unit (SA Instruments, NY, USA). The respiration and body temperature control systems were connected to a computer with pcSam monitoring software (SA Instruments, NY, USA), and these parameters were monitored throughout the acquisition.

The TurboRARE images were acquired in three orthogonal directions (axial, coronal and sagittal) with following parameters: repetition time (TR) = 2500 ms, echo time (TE)

= 33.442 ms, matrix size (256 x 192), field of view = (20 x 20) mm2, 16 slices, slice thickness = 0.5 mm, RARE factor = 8.

Consistent voxel placement for 1H-MRS was achieved in each rat by using anatomical markers such as the external capsule, lateral ventricle, and anterior commissure in three orthogonal RARE slices. While positioning the voxel on the brain, T2-weighted RARE images at three orthogonal position were checked to avoid contribution of cerebral spinal fluid and white matter volume fractions. MAPSHIM was employed to automatically adjust first- and second-order shim coils for the VOI. Spectral line widths of water around 9.8 - 11.7 Hz were obtained. In vivo localised 1H MR spectra were acquired with localisation by Adiabatic Selective Refocusing (LASER) sequence in combination with outer volume suppression (OVS) and VAPOR water suppression (Tkáč *et al.*, 1999; Garwood and DelaBarre, 2001). The following parameters were used: TR = 4000 ms, TE = 20.46 ms, number of averages = 512, water (4.7 ppm) as frequency on resonance, spectral width = 8012.82 Hz, number of acquired points = 2048 yielding a spectral resolution of 1.96 Hz/points. The total acquisition time amounted to ± 34 minutes. Each MRS scan was, during acquisition, dynamically frequency drift corrected. To this end, the water unsuppressed signal was used as an in vivo reference. For each animal, an unsuppressed water signal (TE = 20.46 ms, TR = 4000 ms, 16 averages, scanning time = ± 1 min, water suppression turned off) was acquired immediately after acquiring the water-suppressed spectrum. During post-processing, this unsuppressed water signal was used for Eddy-current correction by the LCModel, where the water-suppressed-MRS signal (in time domain) is point-wise divided by the phase part of the unsuppressed water signal (Mandal, 2012).

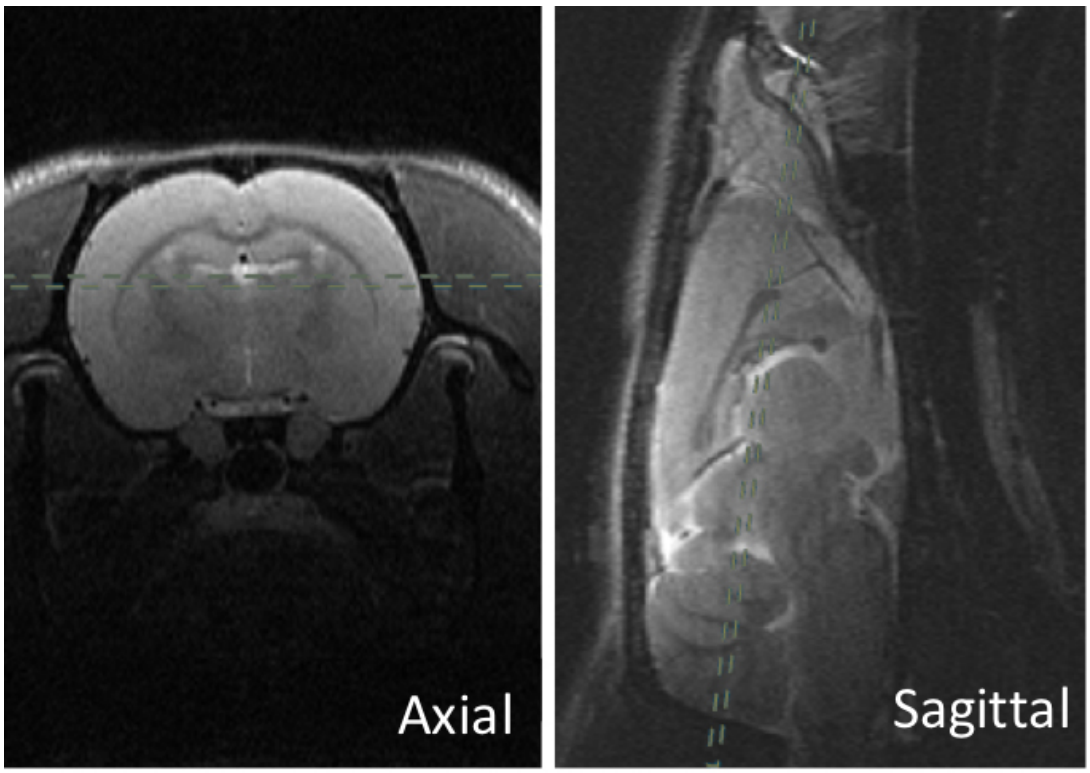

Supplementary Figure 1
The figures depict T2 weighted anatomical images (axial and sagittal). For T2 relaxometry, a single slice is positioned parallel to the cerebral cortex using the anatomical markers (i.e olfactory bulb, cerebral cortex and corpus callosum) allowing the slice to cover the caudate putamen.

3. MR analysis

Due to some presumption of LC model default set up, the concentration units acquired from LC model needed to be corrected to acquire absolute µmol/g unit. LC model default set up assumed that water attenuation factor (ATTH20) 0.7 and metabolite attenuation factor was 1, and NMR visible water concentration of white matter as 35880 mM (tissue water reference based on results of (Ernst *et al.*, 1993)).

To remove the default correction of LC model, first we multipled the concentration output values of LC model with $[(\frac{1}{35880X0.7})]$. After removal of default correction, this value was multipled with water attenuation factor which was calculated using the following formulate ATTH20= exp (-TE/T2). TE and tissue T2 from the current study were used for this estimation. Third, the absolute concentrations of metabolites were corrected for partial volume effects by taking the volume fractions of cerebral spinal fluid, white and gray matter into account in the quantification (Provencher, 1993, 2014). These volume fractions were used to correct the total water concentration for each VOI using the following equation: water concentration = (43300 x fraction gray matter + 35880 x fraction white matter + 55556 x fraction cerebrospinal fluid) / (1-fraction cerebrospinal fluid) (Provencher, 1993). No visible white matter and/or cerebral spinal fluid contribution was detected after inspection of T2 weighted images which were used to localize the MRS voxel. Therefore, in this study the mean water tissue concentrations (from the gray matter) as a reference was assumed as 43300 mM. Since we employed long TR and short TE, correction for relaxation effects of metabolites had minimum effect on metabolite concentration (Provencher, 2014). Therefore, metabolic T1 and T2 relaxation correction was neglected. In addition, T1 relaxation time correction for water attenuation was neglected.

Tissue water T2 relaxation time was estimated using multi slice multi echo (MSME) sequence with following parameters: TR = 2500 ms, TE = 8 ms, number of averages = 1, echo spacing = 8ms, echo images = 20, image size = 256x 192, field of view = 35 mm x 35 mm, slice number = 1, slice thickness = 0.4 mm and acquisition time = 8 min.

Anatomical markers (i.e. olfactory bulb, cerebral cortex and corpus callosum) were used to position the single slice to cover the CP.

4. Immunohistochemistry

Before staining, slides were acclimatized at room temperature during 5 min before being fixed in 4% paraformaldehyde (PFA) during 10 min. They were washed 6 times in PBS (pH 7.4) for 5 min each after which they were immersed in water containing 3% H_2O_2 for 15 min at room temperature to quench endogenous peroxidases. After three washes of 5 min, each in PBS, sections were preincubated with 10% normal donkey serum (NDS) and 0.3% Triton X-100 in PBS at room temperature for 1 h. After 3 washes in PBS for 5 min, the slides were blocked with avidin during 15 min, rinsed briefly and subsequently blocked with biotin during 15 min, followed by incubation with polyclonal mGluR5 primary antibody (1/2500 in PBS with 1% NDS, 10% milk, 0.2% Triton X-100 and 1% BSA; AB5675 Millipore) overnight at room temperature. Subsequently, after three 5 min rinses in PBS, sections were incubated with ExtrAvidin peroxidase 1/1000 for 1 h. After three washes of 5 min each in PBS, the peroxidase reaction was carried out with DAB reagent (Dako) for 2 minutes. The reaction was stopped in tap water. The slides were dehydrated through subsequent immersion in 80%, 95% and two changes of 100% etOH for 5 min each, and finally immersion in two changes of Xylene before mounting with DPX mounting medium (Sigma Aldrich) (Kosten *et al.*, 2016).

5. References

Ernst T, Kreis R, and Ross BD (1993) Absolute Quantitation of Water and Metabolites in the Human Brain. I. Compartments and Water. *J Magn Reson Ser B* **102**:1–8.

Garwood M, and DelaBarre L (2001) The Return of the Frequency Sweep: Designing Adiabatic Pulses for Contemporary NMR. *J Magn Reson* **153**:155–177.

Kosten L, Verhaeghe J, Verkerk R, Thomae D, De Picker L, wyffels L, Van Eetveldt A, Dedeurwaerdere S, Stroobants S, and Staelens S (2016) Multiprobe molecular imaging of an NMDA receptor hypofunction rat model for glutamatergic dysfunction. *Psychiatry Res - Neuroimaging* **248**:1–11.

Mandal PK (2012) In vivo proton magnetic resonance spectroscopic signal processing for the absolute quantitation of brain metabolites. *Eur J Radiol* **81**.

Provencher SW (1993) Estimation of metabolite concentrations from localized in vivo proton NMR spectra. *Magn Reson Med* **30**:672–9.

Provencher SW (2014) LCMODEL & LCMgui User's Manual.

Tkáč I, Starčuk Z, Choi IY, and Gruetter R (1999) In vivo 1H NMR spectroscopy of rat brain at 1 ms echo time. *Magn Reson Med* **41**:649–656.

Watson CC (2000) New, faster, image-based scatter correction for 3D PET. *IEEE Trans Nucl Sci* **47**:1587–1594.